APTARA | JON | jon12408 | Dispatch: October 27, 2016 | CE: AFL
Journal | MSP No. | No. of pages: 12 | PE: Kani Kapoor

Population-Level Correction of Systematic Motion Artifacts in fMRI in Patients with Ischemic Stroke

Q1 Csaba Aranyi, Gábor Opposits, Marianna Nagy, Ervin Berényi, Csilla Vér, László Csiba, Péter Katona, Tamás Spisák, Miklós Emri

From the Department of Medical Imaging, University of Debrecen, Hungary (CA, GO, MN, EB, ME); Department of Neurology, University of Debrecen, Hungary (CV, LC); Department of Diagnostic Radiology, Kenézy Gyula County Hospital, Debrecen, Hungary (PK); and Preclinical Imaging and Biomarker Center, Gedeon Richter Plc., Budapest, Hungary (TS).

ABSTRACT

BACKGROUND: The aim of this study was to reveal potential sources of systematic motion artifacts in stroke functional magnetic resonance imaging (fMRI) focusing on those causing stimulus-correlated motion on the individual-level and separate the motion effect on the fMRI signal changing from the activation-induced alteration at population level.

METHODS: Eleven ischemic stroke patients were examined by fMRI. The fMRI paradigm was based on passive ankle movement on both the healthy and the paretic leg's side. Three individual-level motion correction strategies were compared and we introduced five measures to characterize each subjects' in-scanner relative head movement. After analyzing the correlation of motion parameters and the subjects' physiological scale scores, we selected a parameter to model the motion-related artifacts in the second-level analysis.

RESULTS: At first (individual) level analysis, the noise-component correction-based CompCor method provided the highest $-\log10(p)$ value of cluster-level occurrence probability at 12.4/13.6 for healthy and paretic side stimulus, respectively, with a maximal z-value of 15/16.3. Including the motion parameter at second (group) level resulted in lower cluster occurrence values at 10.9/5.55 while retaining the maximal z-value.

CONCLUSIONS: We proposed a postprocessing pipeline for ischemic stroke fMRI data that combine the CompCor correction at first level with the modeling of motion effect at second-level analysis by a parameter obtained from fMRI data. Our solution is applicable for any fMRI-based stroke rehabilitation study since it does not require any MRI-compatible motion capture system and is based on commonly used methods.

Keywords: Motion correction, fMRI, ischemic stroke, CompCor.

Acceptance: Received May 17, 2016, and in revised form October 17, 2016. Accepted for publication October 17, 2016.

Correspondence: Address correspondence to Csaba Aranyi, Department of Medical Imaging, University of Debrecen, Nagyerdei krt. 98, H-4032 Debrecen, Hungary. E-mail: aranyics11@gmail.com

Acknowledgements and Disclosure: The study was partially supported by the National Brain Research Program ("Charting the normal and pathological macro-scale brain connectome by in vivo neuroimaging," KTIA_13_NAP- A-II/3) and the OTKA 109712 program ("Local hemostatic disorders in the fibrillating atrium"). Special thanks to Rosemary Ellis for her help in preparing the manuscript.

J Neuroimaging 2016;00:1-12.
DOI: 10.1111/jon.12408

Introduction

Stroke is the second cause of mortality and the major cause of permanent disability.[1] The most common motor impairment is the paresis of upper and/or lower limb. The impaired lower limb is a major challenge in the rehabilitation procedure after stroke.

The passive movement is a widely used method in poststroke rehabilitation but the exact mechanism of the improvement method is not yet clarified.[2] The passive movement activates the sensorimotor system that helps to prevent deep venous thrombosis and improves motor function after stroke.[2,3]

Noninvasive mapping of brain activity with blood oxygen level-dependent (BOLD) functional magnetic resonance imaging (fMRI) has become a key technology in many clinical fields, including neuropsychology,[4] neurororadiology,[5] neurosurgery,[6] and radiotherapy.[7] It also has a major role in evaluating poststroke recovery and rehabilitation[8,9] and in investigating the relationship between neural reorganization and functional recovery after stroke.[10] In stroke rehabilitation, the poststroke motor dysfunction and the corresponding potential cerebral reorganization can be characterized by using active and passive movement-based fMRI experiments.[11–16] Although there are a significant amount of studies reporting cortical reorganization related to motor recovery after ischemic stroke,[17–19] similar data for ankle movements are still limited.[13–16]

A crucial problem in fMRI studies is that the measured BOLD signal is highly susceptible to head motion during the acquisition. Therefore, motion correction is a vital step in every work flow during fMRI analysis. The patients' motion in the scanner during the fMRI measurement can be registered by an MRI-compatible motion capture system[20] but this technique is not widely available. In contrast, the image-based, retrospective motion-related artifact removal strategies can be performed without any extra measurement at five different stages of the data processing pipeline: (i) realignment of fMRI images to a reference image (using automatic coregistration approaches);[21] (ii) data-censoring to exclude periods of high motion (scrubbing, despiking);[22,23] (iii) modeling the effect of motion-related parameters on BOLD signal;[24–27] (iv) temporal filtering of time series to discard frequencies encumbered by motion artifacts; and (v) correction for subject-specific motion effects on population level (descriptive summary statistics of subject-specific motion

as second-level model regressors).[28–30] Traditional realignment-based correction approaches ensure that different time points of the BOLD signal correspond to the same position in the brain. However, such methods are not able to handle intensity confounds originating from the establishment of magnetic gradients and subsequent readout of the BOLD signal[31] or spin-history artifacts. Such confounds can be, at least, partially eliminated by nuisance signal regression of BOLD data. The confounder signals can be defined by dedicated physiological monitoring devices during the scan, calculated from motion parameters extracted during spatial realignment-based motion correction or derived directly from the data itself, using a "noise region of interest (ROI)."

According to Satterthwaite et al,[32] between-subject differences of motion are stable, and hence, in-scanner head motion should be considered as a trait. Thus, the effect of the subject-specific spatiotemporal motion pattern on the BOLD signal could bias group analysis when different groups have different tendencies in their spatiotemporal motion patterns. This is particularly problematic in clinical studies when alterations in the BOLD response are associated with a pathological condition causing altered locomotion. In these studies, the variable of interest, both on the individual and the group level, might be correlated with in-scanner motion, which causes systematic error in the analysis and can bias results.

As also shown by Seto et al[33] in an early publication, stimuli-correlated artifacts can especially arise in fMRI experiments with poststroke patients and moreover when investigating fMRI correlates of passive movement of an impaired spastic limb.

The possible neural correlates of in-scanner motion is of high scientific relevance, but hard to investigate. The idea was originally proposed by Yan et al.[34] They detected positive motion-fMRI signal correlation in motor areas, particularly in subjects with low motion. The finding was confirmed by Pujol et al.[35] By contrast, motion-related signal changes were not generally consistent with neural activity in the connectivity studies by Power et al,[22] and Spisák et al[30] who included samples with a relatively large amount of motion. By conclusion, the neural correlates of subject motion, like startling or perception of passive motion is problematic in case of several motion correction techniques, and must be considered during the interpretation of fMRI experiments.

Here, we hypothesize that the degree and predisposition of in-scanner head motion during passive-movement task-based fMRI measurements might be related to clinical symptoms of stroke and corresponding quantitative scales and scores. The purpose of this exploratory study is to reveal potential sources of systematic motion artifacts in stroke fMRI focusing on those of causing stimulus correlated motion on the individual level. Therefore, this study can also be considered as an initial step toward optimizing our fMRI processing pipeline for the investigation of rehabilitation and recovery in poststroke patients.

Methods

Subjects

Functional MRI data from 11 stroke patients (mean time of stroke: 59.3 days [standard deviation, SD = 139.9]; mean age: 64 years [SD = 8.8]; female/male distribution: 6/5) were obtained from a therapeutic study. Patient's demographics data, type, and location of lesion are summarized in Table 1.

Table 1. Demographics, Clinical Characteristics, and Pathology Data of Stroke Patients Involved in This Study

Patient/ Gender	Age (Years)	Lesion Type and Topography (by CT)	Time of Stroke	Severity of Lower Limb Paresis	Plantar Flexion (ROM)	Dorsiflexion (ROM)	MAS Score	NIHSS	mRS
1/Female	61	Cerebral infarct in right MCA region	16 months	Left-sided mild-moderate paresis	35	0	1	1	3
2/Male	63	Cerebral infarct in right MCA region	1 months	Left-sided mild-moderate paresis	25	0	1	1	3
3/Female	65	Cerebral infarct in left MCA	1 months	Right-sided severe paresis	40	5	1	3	4
4/Female	62	Bilateral lacunar infarcts, no fresh lesion	1 months	Right-sided moderate paresis	30	7	0	3	4
5/Male	56	Cerebral infarct in right MCA region	1 months	Left-sided moderate paresis	26	0	3	3	4
6/Male	52	No fresh lesion	9 days	Left-sided moderate paresis	26	5	1	3	4
7/Female	82	Hypodens lesions in right hemisphere	6 days	Left-sided moderate paresis	30	0	2	2	4
8/Female	75	Cerebral infarct in left MCA, old cerebral infarct in right MCA region	12 days	Right-sided mild paresis	30	5	0	2	3
9/Female	71	Lesions frontal horns and cella media in right hemisphere	11 days	Left-sided moderate paresis	32	10	0	2	4
10/Male	59	No fresh lesion	5 days	Right-sided mild paresis	28	10	0	1	2
11/Male	58	No fresh lesion, old lesions in basal ganglia	9 days	Left-sided moderate paresis	35	12	1	2	2

CT = computed tomography; ROM = range of motion; MAS = Modified Ashworth Scale; NIHSS = Institutes of Health Stroke Scale; mRS = modified Rankin scale; MCA = middle cerebral artery.

Table 2. Definitions of Mild and Moderate Paresis and Severe Paresis (Sixth Item of the National Institutes of Health Stroke Scale)

Definition of mild and moderate paresis (sixth item of NIHSS)	1 point	Drift; leg falls by the end of the 5-second period but does not hit the bed
	2 points	Some effort against gravity; leg falls to bed by 5 seconds but has some effort against gravity
Definition of severe paresis	3 points	No effort against gravity; leg falls to bed immediately
(sixth item of NIHSS)	4 points	No movement

NIHSS = National Institutes of Health Stroke Scale.

Clinical Parameters

Patients suffered from moderate or severe lower limb paresis due to ischemic stroke. The definitions of mild and moderate paresis and severe paresis can be seen in Table 2 as described by the National Institutes of Health Stroke Scale (NIHSS). The modified Rankin scale (mRS) was used to classify the degree of poststroke patients' disability (Table 4). The state of subjects was characterized by the Modified Ashworth Scale (MAS) and goniometer measurements (Table 1). Goniometer was used for measuring the passive range of motion degree of ankle plantar and dorsiflexion where the ankle and the hip both were in a neutral position with fully extended knee (90° between the leg and the foot, the hip was not in rotation, see Fig 1). Since the MAS (Table 3) is a quick and easy way to measure spasticity of soleus muscle–which plays an important role in plantar flexion of the foot and maintaining standing position–we determined it by this scale. During soleus muscle tone assessment, the patients were in relaxing supine position keeping their head in alignment at midline and arms close to the trunk. The procedure is designed to maintain the knee joint in a slight flexion between 0° and 45° thereby isolating soleus functions from the undesired contraction of gastrocnemius muscle. By placing one hand on the patient's foot and another on the area above the ankle joint, the examiner performed the passive movement of the ankle joint toward plantar and dorsal flexion with three times repetition.[36]

Table 3. Score Definitions of the Modified Ashworth Scale

MAS	0 point	No increase in muscle tone
	1 point	Slight increase in muscle tone, manifested by a catch and release or by minimal resistance at the end of the range of motion when the affected part(s) is moved in flexion or extension
	2 points	Slight increase in muscle tone, manifested by a catch, followed by minimal resistance throughout the remainder (less than half) of the range of motion
	3 points	More marked increase in muscle tone through most of the range of motion, but affected part(s) easily moved
	4 points	Considerable increase in muscle tone, passive movement difficult
	5 points	Affected part(s) rigid in flexion or extension

MAS = Modified Ashworth Scale.

Table 4. Score Definitions of the Modified Rankin Scale

mRS	0 point	No symptoms
	1 point	No significant disability despite symptoms, able to carry out all usual activities
	2 points	Slight disability, unable to carry out all previous activities, able to look after own affairs without assistance
	3 points	Moderate disability, requiring some help, the ability to walk without assistance
	4 points	Moderately severe disability, unable to walk without assistance, unable to attend to own bodily needs without assistance
	5 points	Severe disability, bedridden, incontinent, requiring constant nursing care, and attention
	6 points	Dead

mRS = modified Rankin scale.

Image Acquisition and Functional MRI Paradigm

Functional and structural images were acquired at the Kenézy Hospital, Debrecen, using a 1.5 Tesla Siemens Magnetom Essenza MR scanner. After the 3-dimensional T1-weighted magnetization-prepared rapid gradient-echo structural image acquisition (echo time [TE] = 4.73 ms, repetition time [TR] = 1,540 ms, inversion time [TI] = 800 ms, flip angle = 15°, 160 slices with .9 × .9 × .9 mm^3 voxels, matrix size = 256 × 200),

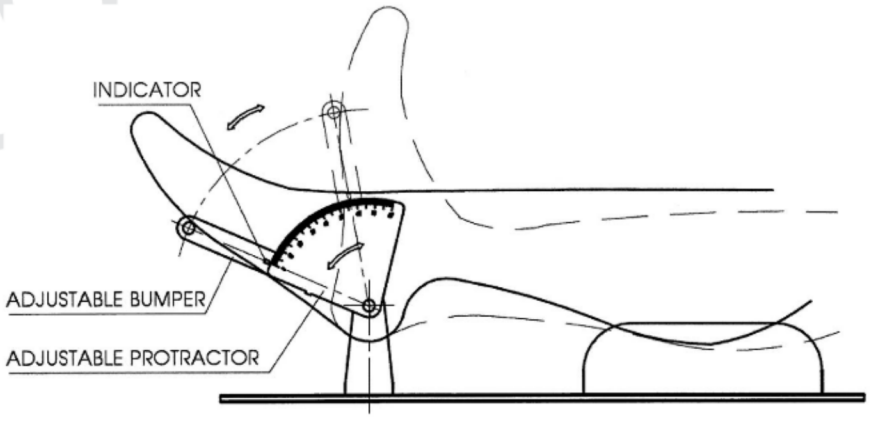

Fig 1. Goniometer measurement of plantar and dorsiflexion ranges. "Range of motion" is a term for the radius of motion achieved by external manipulation without the patient using their own muscles.

the functional images were obtained using a BOLD contrast-sensitive gradient echo EPI sequence (TE = 42 ms, flip angle = 90°, in-plane resolution = 3 × 3 mm^2; volume TR = 4,000 ms, matrix size = 76 × 76). Whole-brain coverage of the functional data was supported by 41 contiguous interleaved 3.3 mm axial slices. Each functional session comprised 100 functional volumes that last 400 seconds containing 40 seconds active and passive alternating blocks beginning with a passive one. In the passive blocks, no stimulus was applied, whereas in the active blocks slow (~1 Hz), passive movement of the left or right feet was performed by the physiotherapist. The activation effect of passive movement of the left and right foot was investigated in separate fMRI sessions. The legs and the hip of the patients were fastened to the bed in order to reduce stimulus correlated head motion.

Image Preprocessing

Before preprocessing in the case of patients with left-hemispheric lesion, the left and the right sides of the structural and functional images were mirrored causing that the stroke side is positioned to the right for all subjects. This step allowed us to perform a pooled population-level statistical analysis for all the patients and avoid splitting the population into two cohorts based on the side of the stroke.

The first three volumes of each functional dataset were excluded from further analysis to avoid T1 equilibrium effect. FMRI time series were motion corrected using the linear realignment utility of FMRIB Software Library (FSL).[37,38] Six motion parameters (three rotation and three translation components of the rigid body transformations) were extracted by the same program.

Brain extraction tool (BET) of FSL was used to remove non-brain areas from both the functional and structural scans.[39] For each fMRI session, a "noise region" was delineated by the analysis of temporal signal-to-noise ratio of BOLD signals and five principal noise components were evaluated for the further component-based noise correction (CompCor) method.[27]

The preprocessed fMRI data were nonlinearly coregistered to the brain-extracted anatomical image and then spatially transformed to the symmetric template of MNI152 space[40] using linear and nonlinear registration utilities of the FSL package,[38] to achieve spatial correspondences for group analysis. An isotropic Gaussian smoothing with 8 mm full width at half maximum was applied on the functional images.

Characterizing In-Scanner Head Movement

Due to intensive head motion that corresponds to the passive movement task, BOLD signals are encumbered with stimulus-related motion artifacts that cannot be easily filtered. A temporal parameter of motion was computed from the relative root-mean-squared (RMS) displacement (Fig 2) that is estimated by the FSL linear image registration tool (FLIRT) using the six computed motion parameters.[37] It characterizes the frame-to-frame deviation between the brain positions over scans. Before analyzing group mean activations, we introduced five measurements to characterize each subject's in-scanner head movement:

1. RMS.scan: the integrated value of RMS curve throughout the whole session:

$$RMS.scan = \sum RMS\,[session]\,.$$

2. RMS.task: the integrated value of RMS during the active blocks:

$$RMS.task = \sum RMS\,[active]\,.$$

3. RMS.rest: the integrated value of RMS curve during the passive blocks:

$$RMS.rest = \sum RMS\,[passive]\,.$$

4. RMS.diff: defined as the test statistic of the Wilcoxon rank-sum test (or Mann-Whitney U-test) with the two samples being the frame-to-frame displacement values in all active and all passive periods. Since the normality test did not provide significant evidence if the samples are normally distributed, we used this method instead of a two-sample Student's *t*-test. Similarly to the Student's *T*-value, the *U*-value has a monotonic relation to the differences between the two samples, namely, the amount of the motion during the active and passive periods.
5. RMS.dyn: the ratio of RMS.task to RMS.rest. This measurement is useful when we focus on motion artifacts induced by the stimulus as it only occurs during the active periods:

$$RMS.dyn = \frac{RMS.task}{RMS.rest}.$$

The monotonic (nondefinitely linear) relationships between the evaluated RMS parameters of the paretic side stimulation and the clinical data were described by Spearman's rank correlation coefficients.

Applied Motion Correction Strategies on Individual-Level Analysis

Three subject-level motion correction strategies were applied during the first-level analysis (hereinafter referred to the abbreviations below):

(a) REG: registration-based motion correction to reestablish the temporal voxel-to-voxel correspondence including temporal filtering of BOLD-signal data with a 100 seconds high-pass filter cutoff.
(b) REG + M6: performing registration-based motion correction and using the six motion parameters estimated during the registration-based motion correction as "Nuisance Explanatory Variables" in general linear model (GLM),[41] in order to account for intensity artifacts such as spin history.[31]
(c) REG + CompCor: registration-based motion correction and component-based noise correction method as described in Ref. 27. A "noise region" was defined on each session of the fMRI imaging data by selecting voxels with high temporal signal-to-noise ratio (the top 10 percentiles in each slice). Then, five noise components identified by principal component analysis were applied as "Nuisance Explanatory Variables" in the GLM.

The preprocessed fMRI data were analyzed within a GLM framework using the FSL Feat software tool.[38] In the voxel-wise GLM, we incorporated the following explanatory variables: (i) the hypothesis for the stimulus according to the block design experiment the temporal derivative of it to allow slight variations in timing (REG), (ii) according to the applied artifact correction technique, further explanatory variables are contributed to the noise: the six motion parameters (REG+M6), or (iii) the five principal noise component time courses based on the noise correction analysis (REG+CompCor). The predictor of interest (the explanatory variable modeling the stimulus blocks) was convolved with the canonical double-gamma hemodynamic response function.[42]

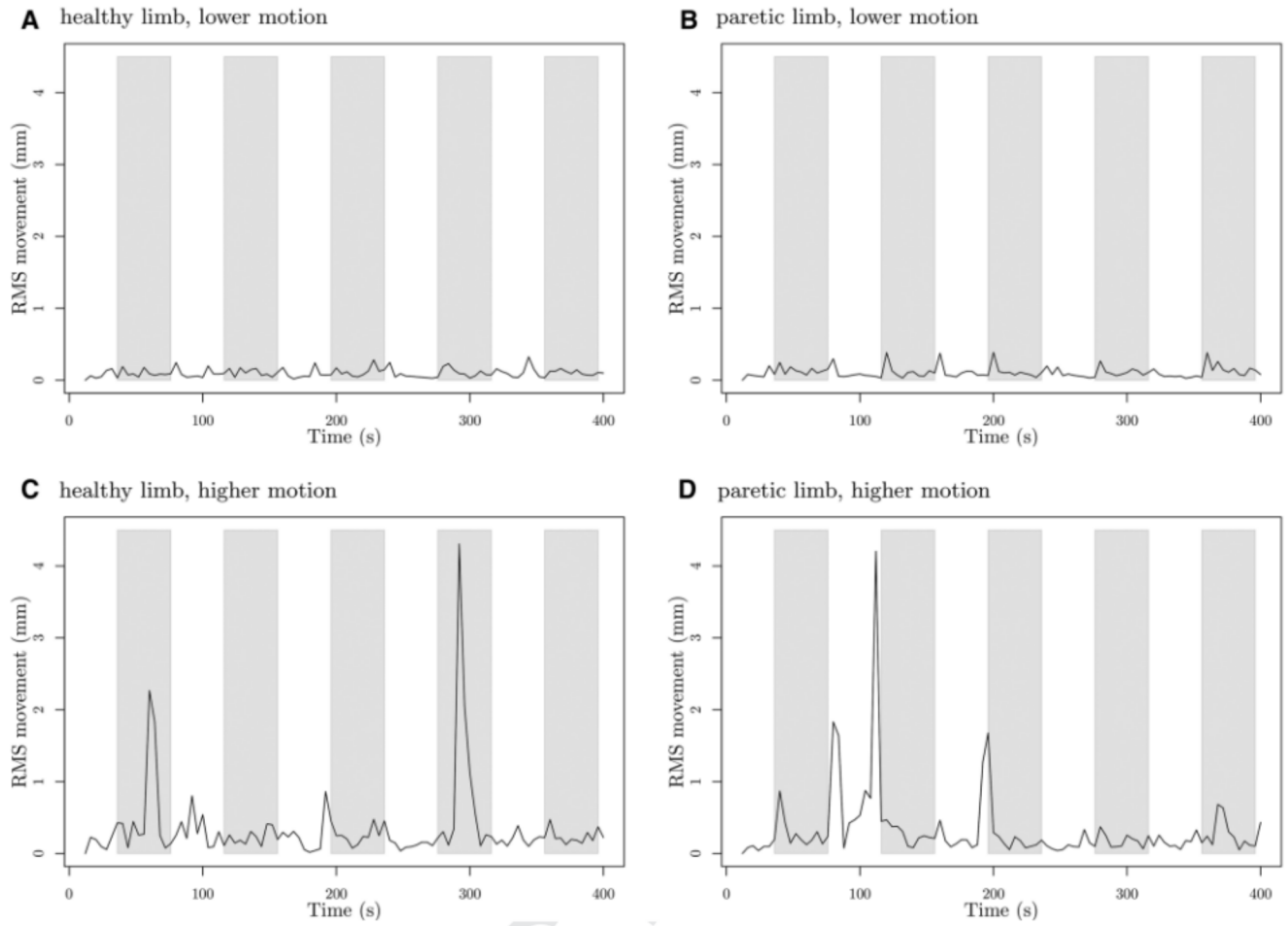

Fig 2. Examples of stimulus-correlated motion. The relative root-mean-squared (RMS) movement is plotted throughout the length of the scan in the case of less motion (top row) and a more moving subject (bottom row). The 40-second-long rest and task periods are highlighted by white and gray bars, respectively. In many cases, significant motion overlapped with the start, or the end of the task sections. The amount of motion artifacts is subject-specific, which may be related to the immobilization caused by stroke.

Population-Level Analysis

The evaluated individual statistical parametric maps were analyzed on population level with two second-level fixed-effect models corresponding to the paretic side and healthy side stimulation. Since some authors published evidences regarding the usefulness of artifact correction on the population level,[29,30] we investigated two techniques during the second-level analysis on either side stimulation:

(a) STIM: stimulus group-mean model, no additional artifact-correction parameter was used on the second-level.
(b) STIM+RMS.diff: stimulus group-mean model extended with RMS.diff parameter (the statistical difference of RMS motion in passive and active blocks) as second-level covariates in the population-level GLM analysis in order to detect and attenuate the effects of false activations related to motion.

Other RMS parameter describing in-scanner motion was not included in the second-level analysis because we were interested in motion parameters that measured the difference of head motion in different blocks (i.e., rest and active). We selected the RMS.diff parameter for modeling the motion effect in second-level GLM because it showed good monotonic relationship with the subjects' plantar and dorsal flexion range and these latter data with low values may cause higher motion artifacts during passive ankle movement of the paretic leg as explained later (Fig 3).

For further analysis, we defined a contrast for creating population mean effect activation patterns and another contrast for evaluating the motion effect parametric images. These activation maps then were rendered by cluster thresholding technique using $z > 2.3$ threshold with the clusters of voxels being significant with $P < .05$.

Results

RMS-Parameter Selection

For selecting a suitable in-scanner head movement parameter for second-level analysis, we investigated the Spearman's rank correlation coefficients between the five introduced RMS-parameters (RMS.scan, RMS.rest, RMS.task, RMS.diff, and RMS.dyn) and the clinical data of subjects (age, plantar flexion, dorsiflexion, MAS, NIHSS, and mRS). The evaluated correlation coefficients were arranged into a matrix (Fig 3) using corrplot R-package.[43] We focused on the correlation values of the goniometer parameters because they measure the passive ankle plantar and dorsiflexion motions range's degree. High correlation value with these parameters indicates which RMS-parameters may be useful for describing the

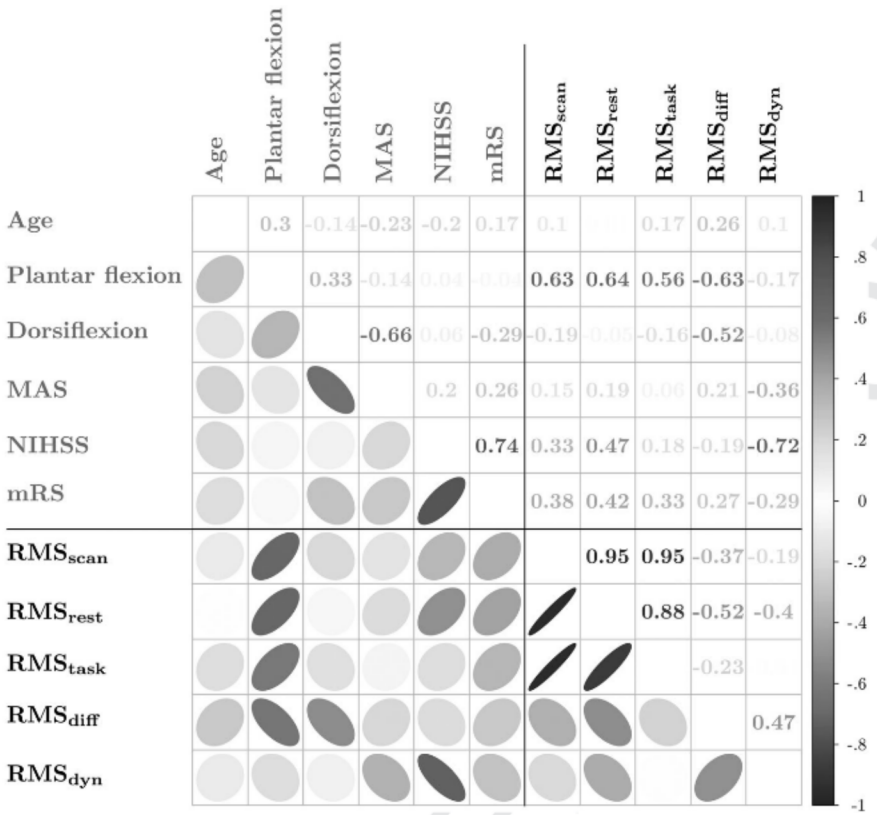

Fig 3. Relations between the introduced motion parameters based on root-mean-squared (RMS) displacement (RMS.scan = total movement, RMS.task = movement during task, RMS.rest = movement during rest, RMS.diff = statistical difference of movement during active and passive periods, RMS.dyn = ratio of movement during task and rest periods) and clinical data (Age, Plantar and dorsal flexion ability, MAS = Modified Ashworth Scale, NIHSS = National Institutes of Health Stroke Scale, mRS = Modified Rankin scale) of stroke in the case of paretic leg movement. The upper triangle of the correlation matrix contains the Spearman's rank correlation coefficients of the appropriate parameters. The lower triangle contains the symbolic representation of these values: the color and the width of the ellipses are related to the absolute value of correlation coefficients and the direction of the slope demonstrates the sign of this value. Plantar flexion shows the highest correlation with the cumulative parameters of movement (RMS.scan, RMS.task, and RMS.rest), which means that we can expect higher in-scanner movement when the ankle's range of motion is higher. However, the statistical difference of motion in active and passive periods (RMS.diff) negatively correlates with this clinical parameter. We interpret this connection as flexing the more immobilized limb causes more involuntary movement of the patient, resulting in more stimulus-correlated motion artifacts. The RMS.dyn ratio of movement in the active blocks to the passive blocks also has significant relationship with NIHSS score.

relationship between the patient's pathological condition and their in-scanner movement. The correlation analysis revealed a strong correlation on the paretic side stimulus between RMS.diff with plantar and dorsal flexion, with correlation coefficients $r = -.63$ and $r = -.52$, respectively, and so we selected this parameter for the further analysis. For demonstration, Figure 4 shows the correlation plots of RMS.scan and RMS.diff parameters.

Comparing the Activation Patterns

Using three different motion correction procedures at first level (REG, REG+M6, REG+CompCor) and two GLM models (STIM, STIM+RMS.diff) at second-level analysis, we compared the parameters of the activation patterns calculated form fMRI data of passive ankle movement stimulation executed on paretic and healthy sides as well. In all cases, BOLD response to passive movement was detected in the primary motor (M1) and supplementary motor areas (SMAs). Each M1/SMA activation cluster was characterized by its volume in cm^3 (V), the cluster-level occurrence probability (p), and its negative log-transformed value ($-\log10(p)$), referred as "co" or "cluster occurrence" later on, the cluster maximum value (z-max) and its spatial position in the MNI152 space (x,y,z). The relationships between these parameters and the fMRI postprocessing methods are shown in Table 5.

Comparing the results of the standard population-level analysis (STIM), we found that the REG+CompCor noise correction method resulted in noticeably higher cluster sizes occurring with higher significance compared to the standard method REG in case of healthy and paretic side stimulation as well. However, using the six motion parameters for REG+M6 technique, no significant activation clusters were found; therefore, we excluded this method from further analysis. The performance of the individual-level techniques is shown in Figure 5 for a typical subject with high in-scanner motion. Inserting the RMS.diff parameter into the GLM model (STIM+RMS.diff), we also observed significant clusters with smaller size and lower logarithmic cluster occurrence probability on both sides (Table 5 bold rows). The most significant changes in cluster statistics were experienced on the paretic side analysis, as we can notice a major decrease in cluster occurrence value at 5.55, using RMS.diff as a second-level covariate, compared to the 13.6 value with the standard model. Also, the volume of the activation cluster is reduced from 66.2 to 19.6 cm^3. This was caused by the merging of

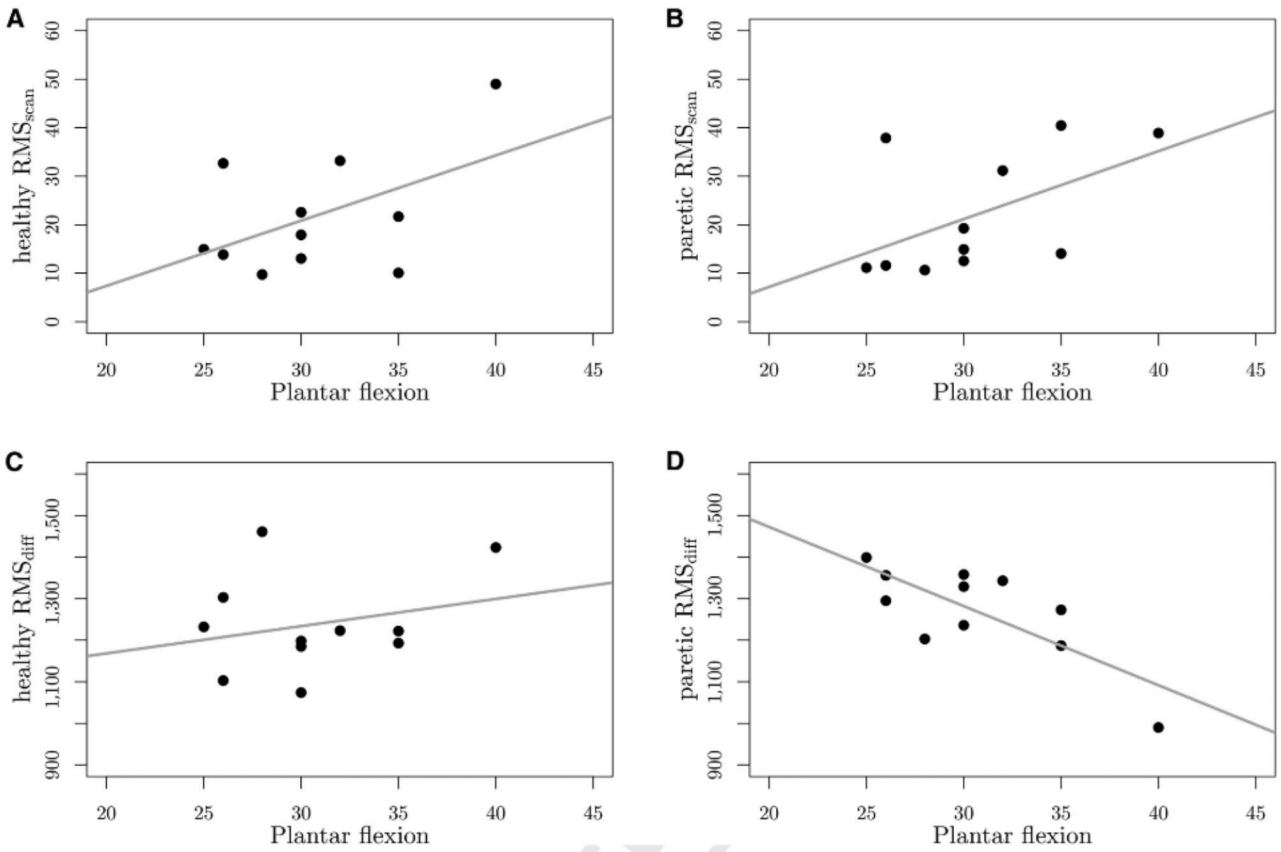

Fig 4. Relationship between the plantar flexion and two stimulus-correlated head motion parameters: the total root-mean-squared motion throughout the functional MRI session (RMS.scan) and the statistical difference of motion in the task and rest periods (RMS.diff). The RMS.scan highly correlates with the plantar flexion ability during healthy (A) and paretic side (B) stimulation, as well. In contrast, the correlation between the RMS.diff and plantar flexion differs in the case of healthy (C) and paretic passive movement (D) since on the paretic side, this correlation is negative.

two simultaneously activated areas of the primary somatosensory cortex (S1) and the secondary somatosensory cortex (S2). These activation clusters were separated by the analysis that included RMS.diff as a nuisance variable that well demonstrates that this model can eliminate the motion correlated voxels from the activation pattern.

In the STIM+RMS.diff model, we also investigated whether the RMS.diff variable accounts for a significant amount of

Table 5. Statistical Analysis of the Healthy and Paretic-Side Ankle Movement Sessions

limb	First Level	Second Level	V	p	−log10(p)	z-max	z-max X (mm)	z-max Y (mm)	z-max Z (mm)
healthy	REG	STIM	18.5 cm^3	.02010	1.7	17.6	−3	−32	70
		STIM + RMS.diff	22.1 cm^3	.00827	2.08	17.4	−3	−32	70
	REG + M6	STIM	8.2 cm^3	1.00000	0	11.976	−2	−30	69
		STIM + RMS.diff	NA	NA	NA	NA	NA	NA	NA
	REG + CompCor	STIM	68.1 cm^3	<.00001	12.4	15	−4	−26	71
		STIM + RMS.diff	55.7 cm^3	<.00001	10.9	15	−3	−30	69
paretic	REG	STIM	20.8 cm^3	.03360	1.47	13.5	5	−31	71
		STIM + RMS.diff	12.8 cm^3	1.00000	0	13.325	5	−31	70
	REG + M6	STIM	51.8 cm^3	1.00000	0	7.875	9	−37	77
		STIM + RMS.diff	NA	NA	NA	NA	NA	NA	NA
	REG + CompCor	STIM	66.2 cm^3	<.00001	13.6	16.3	8	−37	78
		STIM + RMS.diff	19.6 cm^3	<.00001	5.55	16.6	8	−37	78

The column first level indicates the names of subject-level motion correction strategies (REG, REG+M6, REG+CompCor). The results show the group-level analysis of M1/SMA activation cluster with no artifact-correction parameters (STIM), and with RMS.diff as second-level covariates (STIM+RMS.diff). The activated clusters are described by their volume (in cm^3), cluster-level occurrence probability p, the negative log-transformed value of it, and the maximum value and position of cluster z-value in MNI152 space. Among the applied motion correction strategies, CompCor is found to be the most robust. We excluded the statistical analysis of REG + M6 method with covariates, as this motion correction strategy lacks the robustness of other methods for our data. REG = registration-based motion correction; M6 = six motion parameters; CompCor = component-based noise correction; STIM = stimulus group-mean model with no additional artifact-correction parameter; RMS.diff = statistical difference of root-mean-squared motion; NA = not available.

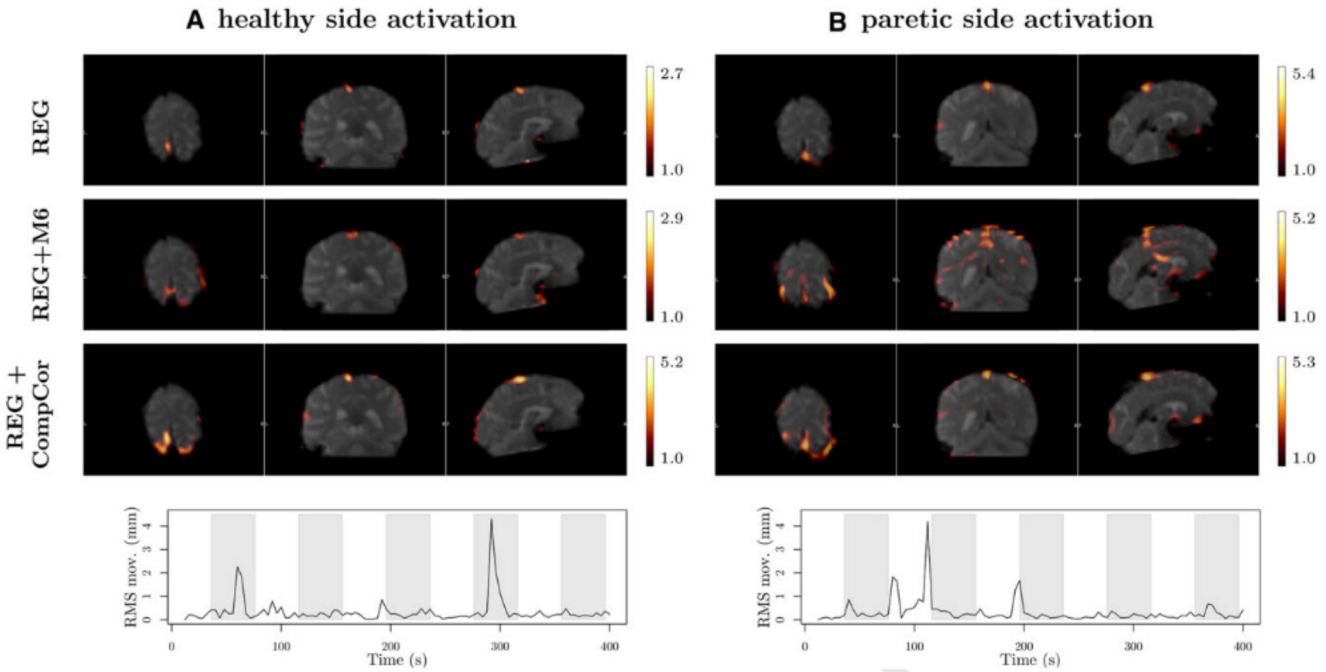

Fig 5. Comparison of the effect of different motion correction techniques at individual-level analysis demonstrated on the activation patterns of a typical patient with high relative (frame-to-frame) root-mean-squared (RMS) in-scanner motion. The orthogonal sections of the activation maps generated by the registration-based uncorrected model (REG) using only realignment of functional MRI images, and the corrected models that include the six motion parameters (REG+M6) or five noise components (REG+CompCor) are shown in the top, middle, and bottom rows, respectively, for the healthy (A) and the paretic leg movement (B). The activation cluster's "cluster occurrence values" (co = −log10(*p*)) are also indicated. The slices are created in the subject's native space.

artificial group-level variability. In the case of the paretic side stimulation, we found that the M1/SMA cluster contains high motion-correlated values. We observed similar but smaller effect in the healthy side stimulation as well (Table 5, Fig 6). Using the introduced RMS.diff parameter in the STIM+RMS.diff model, we were able to separate the motion effect from the real stimulation as illustrated in Figure 7.

Discussion

In this study, we investigated motion correction strategies for fMRI at individual-level analysis, and we introduced a technique to account for patient head movement at population level. A detailed overview of the processing pipeline is visualized in Figure 8. We found that using the six motion parameters from fMRI image registration, the loss of information is significant; therefore, obtaining better activation was not feasible.[30] However, using CompCor as the motion correction method, we achieved highly significant activation clusters.

We propose two new measurements of stimulus-correlated in-scanner head motion for task-based fMRI studies: RMS.diff and RMS.dyn. Our exploratory analysis revealed that some clinical scores of stroke may cooccur with alterations in subjects' kinetics, causing altered in-scanner head motion during passive ankle movement task-based fMRI. We found a strong negative relationship between RMS.diff and two clinical scores that are related to the ability of ankle movement: plantar flexion and dorsiflexion. This may be a systematic connection in ischemic stroke studies where movement of a limb is involved in the task-based fMRI examination. Lower plantar and dorsal flexion of the ankle means lesser ability to move patients' legs causing more in-scanner movement during the task. We also found that RMS.dyn has a strong correlation with another physiological scale parameter, the NIHSS.

Our analysis investigating the population-level effects of RMS.diff on BOLD activation revealed a widespread, strongly significant relationship confirming the confounding effect of stimulus-correlated motion in task-based fMRI analysis. It is known that different groups of subjects can have different amount of movement based on the stimulus resulting in various confounds on the data, which we have to consider and it is particularly challenging to reduce motion artifacts in stroke.[33] We assume that during activation, stimulus-correlated motion effects can either amplify or interfere with neural activity. Thus stimulus-correlated motion might cause false-positive activation in task-based fMRI and the extent of motion artifacts will not be equally distributed throughout the population. This might appear as a systematic error in fMRI studies investigating the neural correlates of the above-mentioned clinical stroke parameters and introduce a bias in the analysis.

Our results confirm that the CompCor individual-level artifact regression technique can effectively reduce the artificial signal components. However, the population-level effect of RMS.diff remains significant even after CompCor, which points to the conclusion that this nuisance signal regression is not able to fully remove this kind of artifact. Here, we propose a population-level correction method: using RMS.diff as a confound regressor in the second-level analysis. Naturally, this method gained smaller activation clusters with lower occurrence levels while retaining the strength of the activation in the M1/SMA cluster (Fig 7), especially regarding the paretic leg. The *Z*-score map for the intersubject variability of RMS.diff suggests higher motion effect in the paretic ankle movement

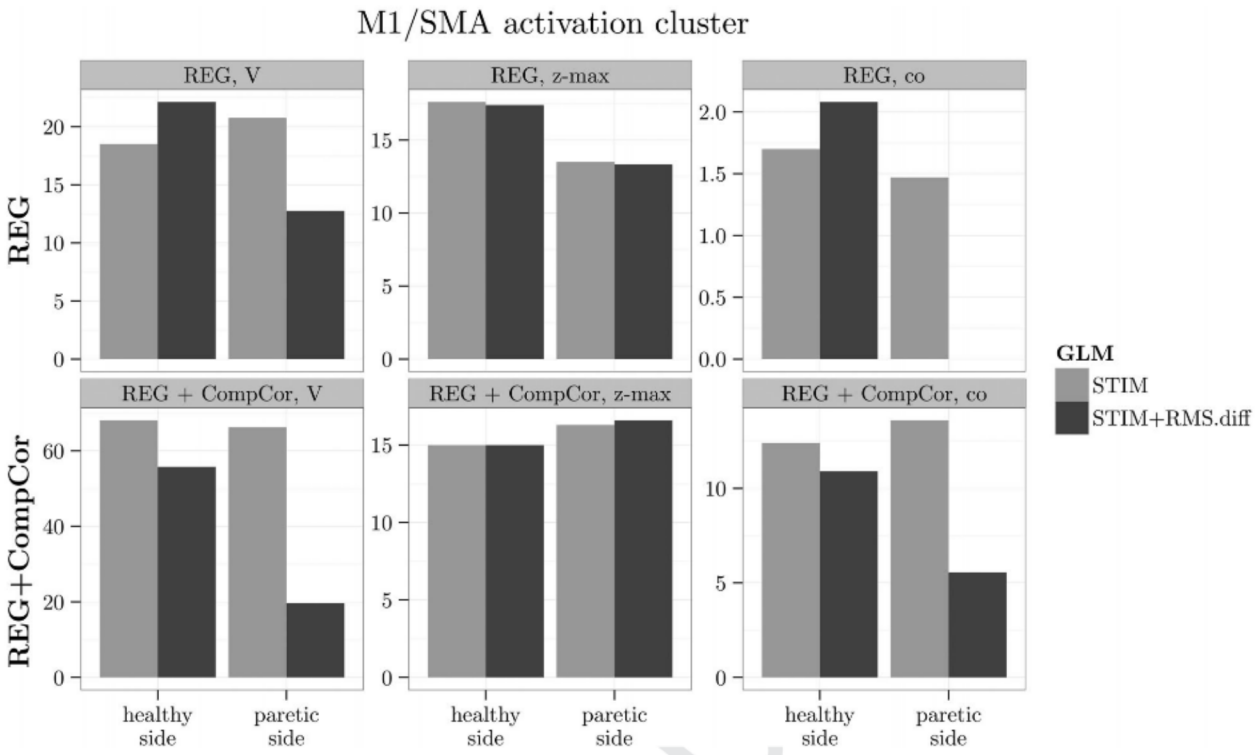

Fig 6. Effects of modeling of a motion parameter on population-level blood-oxygen-level-dependent response of the primary motor cortex and supplementary motor area cluster (M1/SMA) during the healthy and the paretic ankle movement. The results of the registration-based uncorrected model (REG) are compared to the model using noise component correction (REG+CompCor). The columns show the volume of the significantly activated cluster in cm^3 (*V*), the maximal *z*-value in the cluster (*z*-max), and the $-\log10(p)$ cluster-level occurrence probability (co). The color of the bars indicates the applied general linear model (GLM) for stimulus group-mean model without correction (STIM) and with RMS.diff (the statistical difference of root-mean-squared motion between leg movement and passive periods) as a confounder variable (STIM + RMS.diff).

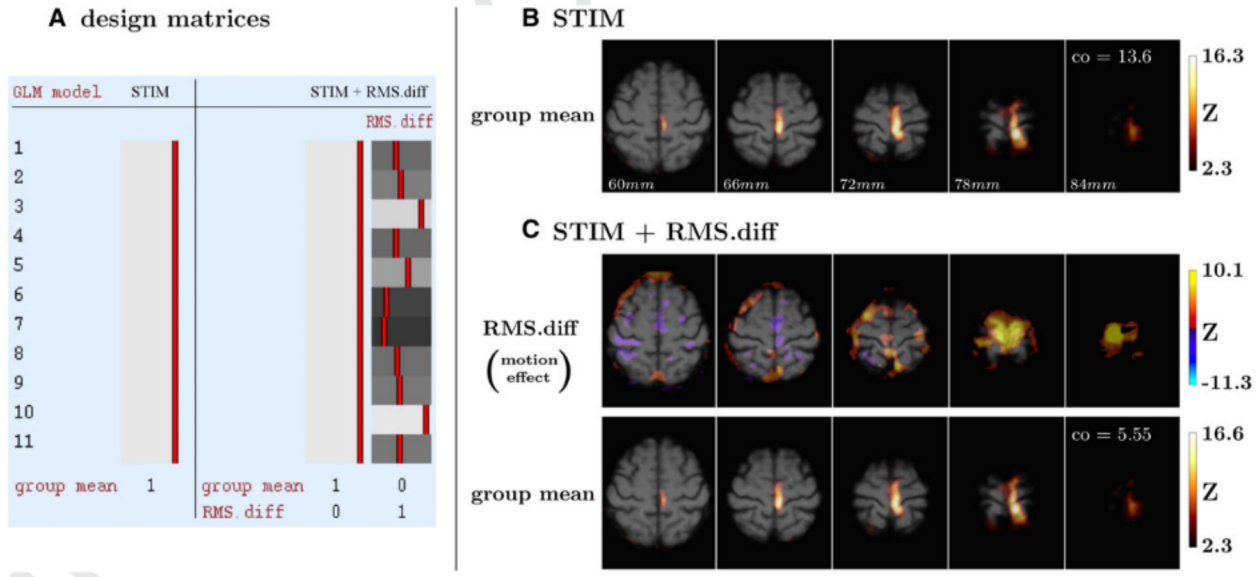

Fig 7. Effects of the population-level motion-correction strategy on mean fMRI activation maps of passive ankle movement of the paretic leg, derived from the subject-level noise-component-based artifact correction method (CompCor). (A) On the left side, the general linear model (GLM) design matrices of the population-level methods are shown to describe the uncorrected stimulus group mean (STIM) and, by modeling intersubject motion variability with the statistical difference of root-mean-squared motion between task and rest periods (RMS.diff), the corrected (STIM+RMS.diff) models. (B) The group mean activation pattern without population-level artifact correction is visualized. (C) The group mean activation map on the bottom was obtained by the motion-corrected model, where RMS.diff was used as the confounder variable as shown in the (A) panel. This is visibly similar to the activation map of the STIM model. However, as presented in Figure 6 and Table 5, cluster size and $-\log10(p)$ cluster-level occurrence probability (co) changes significantly, possibly caused by the correction splitting the activation cluster in the primary motor cortex (M1) apart from the activation observed in the secondary somatosensory cortex (S2). The shown axial slices of brain images are evenly spaced between 60 and 84 mm in the *z*-coordinate of MNI152 space.

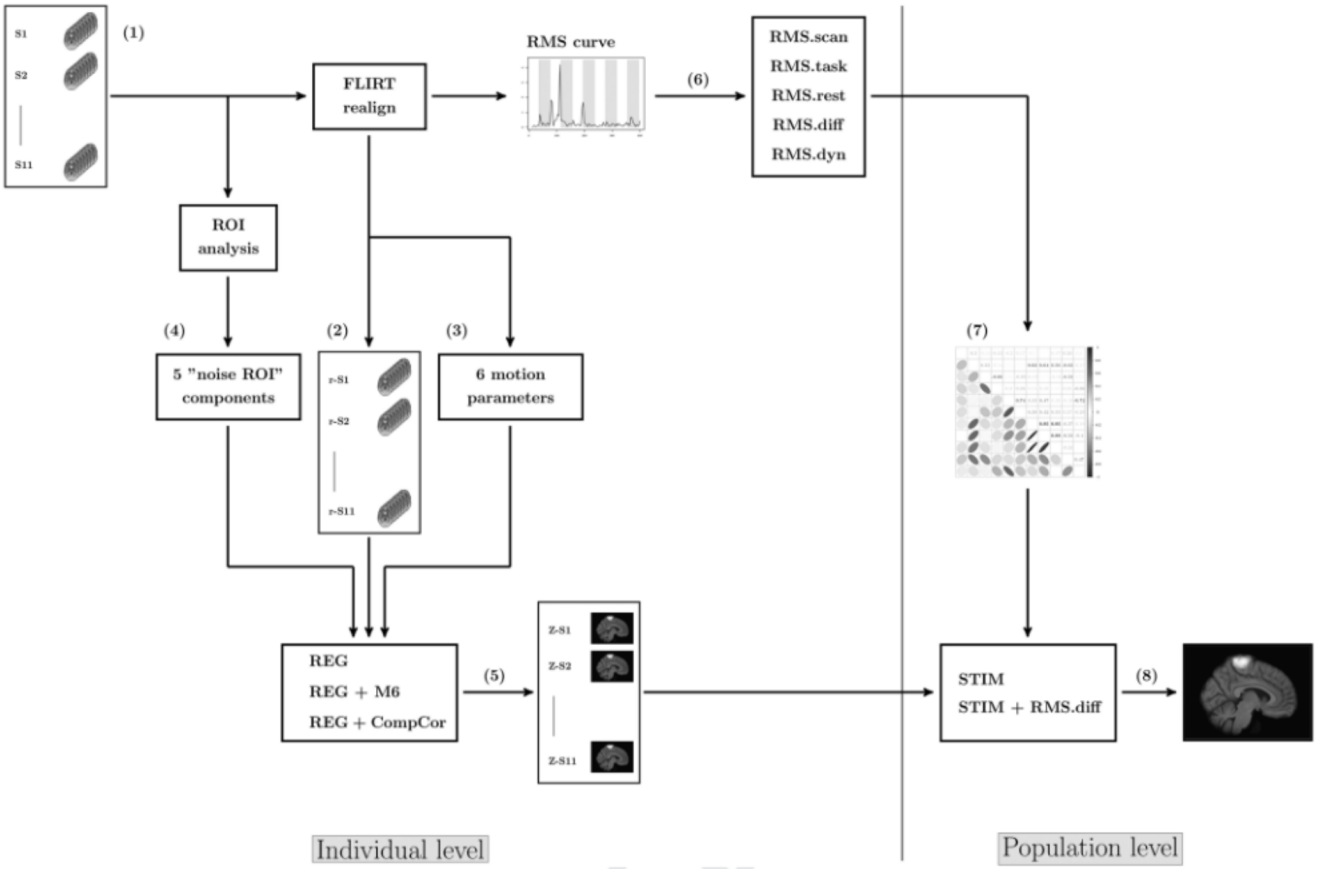

Fig 8. Overview of the functional MRI processing pipeline. The images of the original fMRI series of each subjects (1) are first registered to each other, to reduce displacement of the brain volume throughout the session. This realignment is performed by FLIRT, and produces a realigned series of fMRI images (2), and six motion parameters to account for in-scanner head motion (3). At the same time, region of interest analysis was performed on a selected "noise ROI" of each session to apply noise reduction in the individual-level (first level) statistical analysis (4). The obtained activation maps from the uncorrected (REG), motion corrected (REG + M6), and noise-component-corrected (REG + CompCor) models (5) are used for second-level statistics. To include motion correction in the standard stimulus group-mean model (STIM), numerous measures of motion were defined based on the relative (frame-to-frame) RMS displacement of the brain (6). This includes cumulative (RMS.scan, RMS.task, and RMS.rest) and statistical (RMS.diff, RMS.dyn) parameters. After a correlation analysis between patients' physiological scores and motion parameters (7), we have selected RMS.diff to represent intersubject motion variability in the corrected population-level model (STIM + RMS.diff) (8). REG = registration-based motion correction; M6 = six motion parameters; CompCor = component-based noise correction; STIM = stimulus group-mean model; RMS = root-mean-squared; RMS.scan = total displacement through the session; RMS.task = movement during task; RMS.rest = movement during rest; RMS.diff = statistical difference between head motion during active and passive periods; RMS.dyn = ratio of movement in task and rest periods; ROI = region of interest; FLIRT = FMRIB's Linear Image Registration Tool.

session. A plausible explanation for the reduced cluster size might be that the RMS.diff explained artifactual variance in the model, so without this correction, the analysis may result in a false-positive pattern. Thus, the RMS.diff should be (one of) a parameter that could model the motion effect at the population-level analysis.

As one would expect, analysis of the paretic side was more sensitive to motion correction strategies due to the fact that the data can be more confounded by motion artifacts as opposed to the healthy side. Using RMS.diff together with CompCor as an individual-level motion correction technique might be more effective in reducing the biasing effect of stimulus-correlated motion and might help in avoiding false positives when investigating neural correlates of stroke with task-based fMRI.

To conclude, the possible neural correlates of in-scanner motion are indeed a problem while interpreting results of fMRI experiments. The same applies to the method introduced in the current study. However, the positive response to large stimulus-correlated motion is typically located over tissue boundaries in our study (as shown in Fig 7), which is characteristic to motion artifacts.[26] Negative relationship with RMS.diff was also observed mainly at the gray–white matter boundary, which is not likely to reflect response of neural origin. Thus, the neural correlates of RMS.diff should be negligible compared to the consequences of motion artifacts. Nevertheless, this effect cannot be fully excluded, neither for the proposed method, nor in the case of widely used CompCor correction or several other techniques, and should be applied carefully.

Conclusion

We proposed a postprocessing pipeline that combines the CompCor correction at first level with the modeling of motion effect at second-level analysis by a parameter obtained from fMRI data for ischemic stroke studies.

Here, we demonstrated that stimulus-correlated motion artifacts in passive-movement task-based fMRI measurements are related to clinical symptoms of stroke and corresponding quantitative scales and scores. These motion artifacts might appear as a systematic confound in studies where the neural correlates of stroke rehabilitation are investigated.

Here, we proposed RMS.diff as a parameter that quantifies stimulus-correlated motion for each subject and can be effectively incorporated into the population-level analysis as a confound effect. As a result, a widespread significant relationship between RMS.diff and fMRI BOLD response was observed. This points to the conclusion that even after applying state-of-the-art subject-level signal regression-based artifact-correction techniques, a significant motion-related artificial variance remains in the population-level fMRI activation pattern data.

At the same time, modeling the individual amount of stimulus-correlated motion in the population-level model by RMS.diff may be considered as group-level correction technique, since it is, at least partly, able to account for this artificial variability. An advantage of this technique is that it does not require any MRI-compatible motion capture system and it is based on commonly used software and mathematical methods.

However, correlating neural activity with clinical symptoms and rehabilitation progress in stroke patients still might be confounded by stimulus-correlated motion artifacts. Separating activation of neural and artificial origin is not fully possible. Thus, group comparisons where the variable-of-interest is correlated with the degree of stimulus-correlated subject motion must be performed with caution.

References

1. Vér C, Hofgárt G, Menyhárt L, et al. Ankle-foot continuous passive motion device for mobilization of acute stroke patients. Open J Ther Rehabil 2015;3:23-34.
2. Lindberg P, Schmitz C, Forssberg H, et al. Effects of passive-active movement training on upper limb motor function and cortical activation in chronic patients with stroke: a pilot study. J Rehabil Med 2004;36:117-23.
3. Szameitat AJ, Shen S, Conforto A, et al. Cortical activation during executed, imagined, observed, and passive wrist movements in healthy volunteers and stroke patients. Neuroimage 2012;62:266-80.
4. Logothetis NK, Pauls J, Augath M, et al. Neurophysiological investigation of the basis of the fMRI signal. Nature 2001;412:150-7.
5. Ulmer S, Jansen O. *fMRI Basics and Clinical Applications*. 2nd ed. Springer, 2013.
6. Bobholz J, Rao SM, Saykin AJ, et al. Clinical use of functional magnetic resonance imaging: reflections on the new CPT codes. Neuropsychol Rev 2007;17:189-91.
7. Kovács A, Tóth L, Glavák C, et al. Integrating functional MRI information into radiotherapy planning of CNS tumors-early experiences. Pathol Oncol Res 2011;17:207-17.
8. Eliassen JC, Boespflug EL, Lamy M, et al. Brain-mapping techniques for evaluating poststroke recovery and rehabilitation: a review. Top Stroke Rehabil 2008;15:427-50.
9. Huettel SA, Song AW, McCarthy G. *Functional Magnetic Resonance Imaging*. 2nd ed. Massachusetts: Sinauer, 2009.
10. Calautti C, Naccarato M, Jones PS, et al. The relationship between motor deficit and hemisphere activation balance after stroke: a 3T fMRI study. Neuroimage 2007;34:322-31.
11. Jang SH, Ahn SH, Lee J, et al. Cortical reorganization of sensorimotor function in a patient with cortical infarct. NeuroRehabilitation 2010;26:163-6.
12. Jang SH. Motor recovery mechanisms in patients with middle cerebral artery infarct: a mini-review. Eur Neurol 2012;68:234-9.
13. Ciccarelli O, Toosy AT, Marsden JF, et al. Identifying brain regions for integrative sensorimotor processing with ankle movements. Exp Brain Res 2005;166:31-42.
14. Enzinger C, Johansen-Berg H, Dawes H, et al. Functional MRI correlates of lower limb function in stroke victims with gait impairment. Stroke 2008;39:1507-13.
15. Francis S, Lin X, Aboushoushah S, et al. fMRI analysis of active, passive and electrically stimulated ankle dorsiflexion. Neuroimage 2009;44:469-79.
16. Hollnagel C, Brügger M, Vallery H, et al. Brain activity during stepping: a novel MRI-compatible device. J Neurosci Methods 2011;201:124-30.
17. Rossini PM, Caltagirone C, Castriota-Scanderbeg A, et al. Hand motor cortical area reorganization in stroke: a study with fMRI, MEG and TCS maps. Neuroreport 1998;9:2141-6.
18. Schaechter JD, Kraft E, Hilliard TS, et al. Motor recovery and cortical reorganization after constraint-induced movement therapy in stroke patients: a preliminary study. Neurorehabil Neural Repair 2002;16:326-38.
19. Johansen-Berg H, Dawes H, Guy C, et al. Correlation between motor improvements and altered fMRI activity after rehabilitative therapy. Brain 2002;125:2731-42.
20. Casellato C, Ferrante S, Gandolla M, et al. Simultaneous measurements of kinematics and fMRI: compatibility assessment and case report on recovery evaluation of one stroke patient. J Neuroeng Rehabil 2010;23:7-49.
21. Kim B, Boes JL, Bland PH, et al. Motion correction in fMRI via registration of individual slices into an anatomical volume. Magn Reson Med 1999;41:964-72.
22. Power JD, Barnes KA, Snyder AZ, et al. Spurious but systematic correlations in functional connectivity MRI networks arise from subject motion. Neuroimage 2012;59:2142-54.
23. Satterthwaite TD, Elliott MA, Gerraty RT, et al. An improved framework for confound regression and filtering for control of motion artifact in the preprocessing of resting-state functional connectivity data. Neuroimage 2013;64:240-56.
24. Friston KJ, Holmes AP, Worsley KJ, et al. Statistical parametric maps in functional imaging: a general linear approach. Hum Brain Mapp 1994;2:189-210.
25. Fox MD, Zhang D, Snyder AZ, et al. The global signal and observed anticorrelated resting state brain networks. J Neurophysiol 2009;101:3270-83.
26. Glover GH, Li TQ, Ress D. Image-based method for retrospective correction of physiological motion effects in fMRI: RETROICOR. Magn Reson Med 2000;44:162-7.
27. Behzadi Y, Restom K, Liau J, et al. A component based noise correction method (com567pcor) for bold and perfusion based fmri. Neuroimage 2007;37:90-101.
28. Fair DA, Nigg JT, Iyer S, et al. Distinct neural signatures detected for ADHD subtypes after controlling for micro-movements in resting state functional connectivity MRI data. Front Syst Neurosci 2013;6:80.
29. Siegel JS, Power JD, Dubis JW, et al. Statistical improvements in functional magnetic resonance imaging analyses produced by censoring high-motion data points. Hum Brain Mapp 2014;35:1981-96.
30. Spisák T, Jakab A, Kis SA, et al. Voxel-wise motion artifacts in population-level whole-brain connectivity analysis of resting-state FMRI. PLoS One 2014;9:e104947.
31. Friston KJ, Williams S, Howard R, et al. Movement-related effects in fMRI time-series. Magn Reson Med 1996;35:346-55.
32. Satterthwaite TD, Wolf DH, Loughead J, et. al. Impact of in-scanner head motion on multiple measures of functional connectivity: relevance for studies of neurodevelopment in youth. Neuroimage 2012;60:623-32.
33. Seto E, Sela G, McIlroy WE, et al. Quantifying head motion associated with motor tasks used in fMRI. Neuroimage 2001;14:284-97.
34. Yan CG, Cheung B, Kelly C, et al. A comprehensive assessment of regional variation in the impact of head

micromovements on functional connectomics. Neuroimage 2013;76:183-201.
35. Pujol J, Macià D, BlancoHinojo L, et al. Does motionrelated brain functional connectivity reflect both artifacts and genuine neural activity?. Neuroimage 2014;101:87-95.
36. Blackburn M, van Vilet P, Mockett SP. Reliability of measurements obtained with the Modified Ashworth Scale in the lower extremities of people with stroke. Phys Ther 2002;82:25-34.
37. Jenkinson M, Bannister P, Brady M, et al. Improved optimization for the robust and accurate linear registration and motion correction of brain images. Neuroimage 2002;17:825-41.
38. Jenkinson M, Beckmann CF, Behrens TE, et al. FSL. Neuroimage 2012;62:782-90.
39. Smith SM. Fast robust automated brain extraction. Hum Brain Mapp 2002;17:143-55.
40. Grabner G, Janke AL, Budge MM, et al. Symmetric atlasing and model based segmentation: an application to the hippocampus in older adults. Med Image Comput Comput Assist Interv 2006;9:58-66.
41. Johnstone T, Ores Walsh KS, Greischar LL, et al. Motion correction and the use of motion covariates in multiple-subject fMRI analysis. Hum Brain Mapp 2006;27:779-88.
42. Lindquist MA, Meng Loh J, Atlas LY, et al. Modeling the hemodynamic response function in fMRI: efficiency, bias and mismodeling. Neuroimage 2009;45:S187-98.
43. Friendly M. Corrgrams: exploratory displays for correlation matrices. Am Stat 2002;56:316–24.